



Developing a method to measure actual *CT* distribution in an ozone contactor with a reactive tracer test

Dooil Kim*

Civil and Environmental Engineering, Dankook University, 126 Jukjeon, Yongin, Gyeonggido 406-772, Korea, email: dikim21@dankook.ac.kr

Received 11 January 2014; Accepted 20 June 2014

ABSTRACT

CT (i.e. concentration \times contact time) is one of the critical design and operational parameters to manage pathogen inactivation in ozone treatment. Ozone concentration and contact time are measured using an ozone sensor and a non-reactive tracer test, respectively. The actual *CT* value, however, might be different from this because of non-ideal flow in an ozone contactor. Hence, there is a need to investigate the spatial actual *CT* distribution. We developed a method to quantify *CT* distribution in an ozone contactor using a microsphere and three-dimensional laser-induced fluorescence technology. The dyed carboxylate microsphere, 50 nm in diameter, was used since its fluorescence decreased gradually according to *CT* without turbidity issues. The microsphere was fed continuously into an ozone contactor and reacted with ozone. After reaching steady state, planar laser sheets scanned a model ozone contactor and induced fluorescence light, which was captured with a high-speed video camera. The image was corrected and calibrated to produce fluorescence distribution, which was further processed into *CT* in an ozone contactor. We successfully obtained spatial actual *CT* distribution of a model ozone contactor and identified that *CT* distribution was not uniform in a model ozone contactor because of non-ideal flow.

Keywords: Reactive tracer test; Dyed microsphere; Laser-induced fluorescence; Ozone disinfection; *CT* (concentration \times contact time)

1. Introduction

Ozone is widely used as a disinfectant for drinking water because of its high inactivation efficiency for *Cryptosporidium parvum* oocyst and low-chlorinated disinfection by-product formation [1–3]. However, ozone produces bromate, a disinfection by-product of ozone treatment of raw water rich in bromide and classified as carcinogen in the category 2B by WHO [4,5]. As relatively high ozone exposure is required for

C. parvum oocyst inactivation, ozonation could be incorporated with excessive bromate formation [6].

Disinfection efficiency of a pathogen has been generally estimated by *CT* (concentration \times contact time with ozone) for the design and operation of a water treatment plant. *C* is the average ozone concentration in each chamber and measured from ozone sensors installed in an ozone contactor. The measured ozone concentration could not represent the average concentration exactly because the concentration in each

Presented at the 6th International Conference on the "Challenges in Environmental Science and Engineering" (CESE-2013), 29 October–2 November 2013, Daegu, Korea

chamber would be widely distributed in an ozone contactor. T is the contact time with ozone in each chamber and obtained from a tracer test with non-reactive dye. Since, ozone contact time is affected by non-ideal flow hydrodynamics (i.e. short-circuiting, recirculation, and stagnant zone) in each chamber, actual contact time could not be measured exactly. Hence, T_{10} has been used as an alternative of the actual contact time. T_{10} is defined as time required for 10% of the injected tracer to pass through a reactor and obtained through a non-reactive tracer test. Since, CT_{10} is much smaller than actual CT ; it may lead to over dosing of ozone and additional bromate formation in an ozone contactor.

An ozone contactor with upward and downward flow through multiple consecutive chambers has been used to attain higher T_{10}/HDT since the CSTRs in series have higher T_{10}/HDT value as the number of the CSTRs in series increases [7,8]. HDT is hydraulic detention time and determined by dividing the volume of reactor by flow rate. However, non-ideal flow characteristics incorporated in a full-scale plant could decrease the T_{10}/HDT and result in a lower equivalent number of the CSTRs in series [9,10]. Internal recirculation, stagnant zone, and short-circuiting are major hydrodynamic characteristics causing non-ideal flow in an ozone contactor [9,11–13]. Continuous and circulative flow could hold tracer in an ozone chamber, which could result in tailing and spreading of a residence time distribution (RTD) curve with pulse tracer injection [14]. Thus, non-ideal flow should be avoided so that disinfection efficacy and other advantages such as saving ozone and minimization of disinfection by-product formation could be maximized [15]. Three-dimensional laser-induced fluorescence (3D-LIF) technology was developed to visualize non-ideal flow in an ozone contactor and proved to be a useful tool for observing the hydrodynamic behaviors in an ozone contactor by quantifying spatial tracer concentration in a target ozone contactor [16].

The principles of a 3D-LIF technologies were explained by Tian and Roberts [16]. Briefly, laser dye (i.e. Rhodamine 6G) emits fluorescence light when it is exposed to a laser beam with specific excitation wavelength and enough energy. Rhodamine 6G has an excitation wavelength at 526 nm and fluorescence emission wavelength at 555 nm. Planar laser sheets are created by reflecting a laser beam with oscillating a mirror and collimating with plano-convex lens as shown in Fig. 1. The intensity of fluorescence light is linearly proportional to tracer concentration which ranges from 0 to 50 $\mu\text{g}/\text{L}$ [16]. The planar fluorescence images are captured by a high-speed video camera as shown in the Fig. 1.

The images are further processed to correct optical lens errors (i.e. vignetting) and laser light loss during traveling in the water (i.e. attenuation) [16]. Reduction of brightness at the periphery is called as vignetting which is corrected pixel by pixel using Eq. (1) with standard black and white image [16].

$$I_c(i, k) = K \frac{I_r(i, k) - I_b(i, k)}{I_s(i, k) - I_b(i, k)} \quad (1)$$

where $I_c(i, k)$, $I_r(i, k)$, $I_s(i, k)$, and $I_b(i, k)$ are pixels of corrected, raw, standard white, and black image, respectively, at i th and j th pixel indices. K is the average pixel value of a standard white image. Images are further processed to correct attenuation error, which is corrected with Beer's law shown in Eqs. (2) and (3) [17].

$$P = P_0 e^{-(a_w + 0.00023 \times C)(x - x_0)} \quad (2)$$

$$a = a_w + 0.00023 \times C \quad (3)$$

where P and P_0 are laser intensity at the location x and x_0 , respectively. a_w is an attenuation coefficient of water, which ranges from 0.0011 to 0.0045 cm^{-1} . C is the concentration of Rhodamine 6G. These correction procedures were performed by a software named *TFlook* developed by Tian and Roberts [16]. Tracer concentration was calculated with Eq. (4) from pixel intensity.

$$C = \alpha \times I \quad (4)$$

where C ($\mu\text{g}/\text{L}$) is tracer concentration and I is pixel intensity. α is correlation coefficient.

Visualization of the hydrodynamics of an ozone contactor using 3D-LIF enabled us to look inside of an ozone contactor for effective disinfection system design. In this study, novel technology was developed to visually quantify spatial CT distribution using 3D-LIF system and dyed microsphere. Additionally, the reproducibility of 3D-LIF system with non-reactive tracer was shown with statistical analysis.

2. Methods and materials

2.1. 3D-LIF imaging system

Scanning planar laser sheets are created by reflecting Argon-ion laser beam (1.75 W in power) using two orthogonal axis oscillating scanning mirrors and collimating with plano-convex lens as shown in Fig. 1. Forty laser slices compose a set of spatial scanning

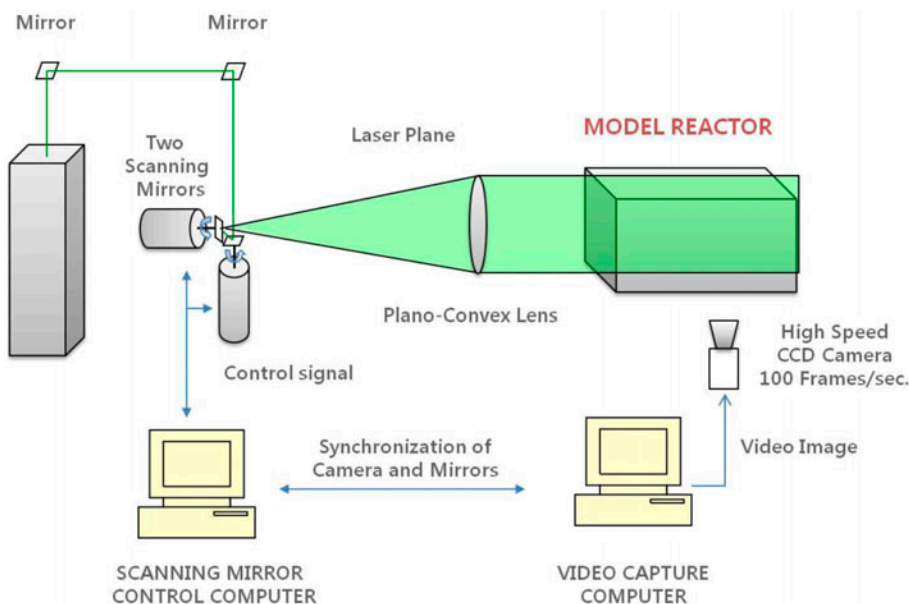


Fig. 1. Schematic diagram of 3D-LIF system.

within 0.41 s. A laser dye (i.e. Rhodamine 6G) in the path of laser slice is excited by the 514 nm laser beam and emits fluorescence light. This planar sheet of fluorescence light is captured using a high-speed video camera at the rate of 100 frame/s with 256 gray levels and then stored in the high-capacity storage device. This video camera is equipped with an image sensor with a resolution of 532 by 526 pixels, lens with 25 mm focal length (Fujinon, Saitama, Japan), and 530 nm filter (Schott glass 530, Reynard Corporation, San Clemente, CA) between lens and image sensor. Captured video images are digitalized by an I/O board and then stored into desktop computer by program called Video Savant™ (IO Industries Inc., London, England).

2.2. Model ozone reactor

A model ozone contactor composed of 12 chambers was made from clear acrylic glass. The dimension and flow rate are shown in Fig. 2. Water flows in upward or downward directions in the model ozone contactor. The dimension of the model reactor was 1,360 mm W × 190 mm H × 230 mm D. The flow rate was ranged from 6 to 18 L/min.

2.3. Non-reactive tracer test with a 3D-LIF system

Conservative tracer tests using 3D-LIF were carried out with a model ozone contactor. De-chlorinated tap water was fed into the reactor at room temperature ($20 \pm 2^\circ\text{C}$). 1–2 mL of laser-dye stock

solution (i.e. 100 mg/L of Rhodamine 6G, Sigma-Aldrich, St. Louise, MO) was pulse-injected directly into inlet of the model ozone contactor using a syringe. Image capture was immediately initiated after dye pulse injection. The images were calibrated and further processed to the input file of the Techplot software (Techplot Inc., Bellevue, WA) using the TFlock software [16]. The concentration change over time at the outlet of each chamber was obtained using the Techplot software.

2.4. Reactive tracer test with nanosized-dyed sphere

A reactive tracer test was performed using dyed microsphere, 50 nm in diameter, (Fluoresbrite® YO Carboxylate Microspheres). The microsphere was purchased from Polyscience Inc. (Warrington, PA). The microsphere was packaged in 2.5% aqueous suspension and had a concentration of 3.64×10^{14} particles/mL. The diameter coefficient of variation (COV) was 15%. Excitation wavelength was 529 nm and the emission wavelength was 546 nm. Four 10 mL bottles of the microsphere were mixed with 500 L tap water and then fed into the model ozone contactor. The microsphere solution was mixed with ozone stock solution at the inlet of the model ozone contactor as shown in the Fig. 2. Initial ozone concentration was set as 0.5 mg/L using ozone stock solution with concentration of 12.3 mg O₃/L. A steady-state flow rate was 6 L/min. The laser intensity was 1.75 W. The video capturing rate was 100 frames/s.

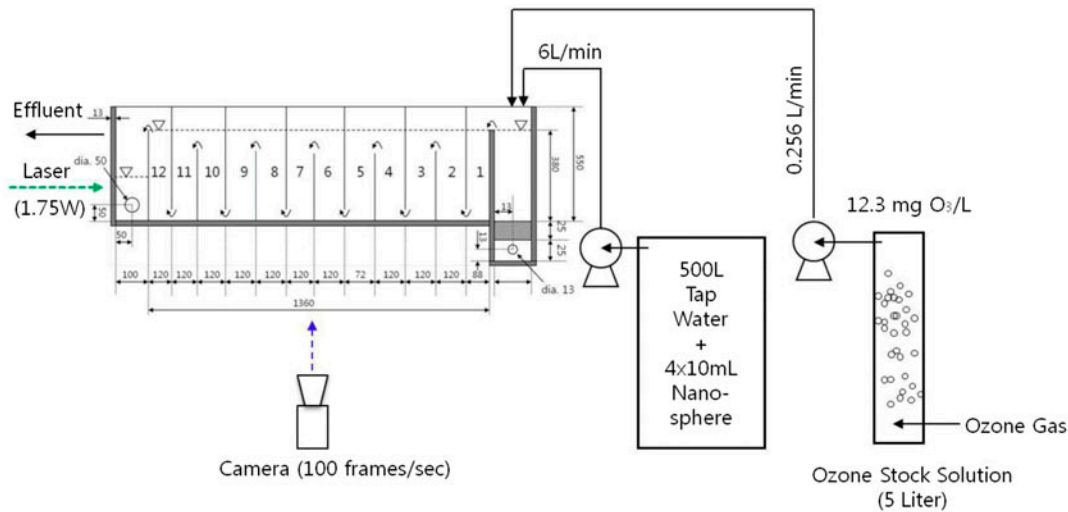


Fig. 2. Schematic diagram of model ozone contactor (unit: mm).

3. Results and discussion

3.1. Non-reactive tracer test with the 3D-LIF

Attenuation is loss of laser light intensity during traveling in water and influences the length of a model reactor significantly. Beer's Law, shown in Eqs. (2) and (3), matched well with 50 $\mu\text{g/L}$ Rhodamine 6G solution after vignetting correction as shown in Fig. 3. The initial pixel intensities (i.e. P_0) before and after vignetting correction were 158 and 155, respectively. The clear water attenuation coefficients (i.e. a_w) before and after vignetting correction were 0.022 and 0.024 cm^{-1} , respectively. Downward peaks in the Fig. 3 were caused by the acrylic reactor baffle which had no Rhodamine 6G inside. The pixel intensity matched slightly better with Beer's law after vignetting correction as shown in Fig. 3. The effect of acrylic material on laser attenuation was shown to be minor. If the acrylic baffle caused significant attenuation, a stepwise decrease would be expected at each baffle from Fig. 3.

A vertical flow ozone contactor, as shown in Fig. 2, bears non-ideal flow characteristics like stagnant zone, internal recirculation, and short-circuiting [18]. These hydraulic characteristics decreases disinfection efficiency and increases operational cost of an ozone contactor. 3D-LIF system showed the existence of non-ideal flow in an ozone contactor [18]. Fig. 4(a) shows the RTD curves using a non-reactive tracer (i.e. Rhodamine 6G) at 14 L/min flow rate. The outlet concentration of each chamber was obtained by surface average concentrations at the exit. The existence of non-ideal flow in the model ozone contactor was clearly identified from the normalized RTD curves as shown in Fig. 4(a). Note

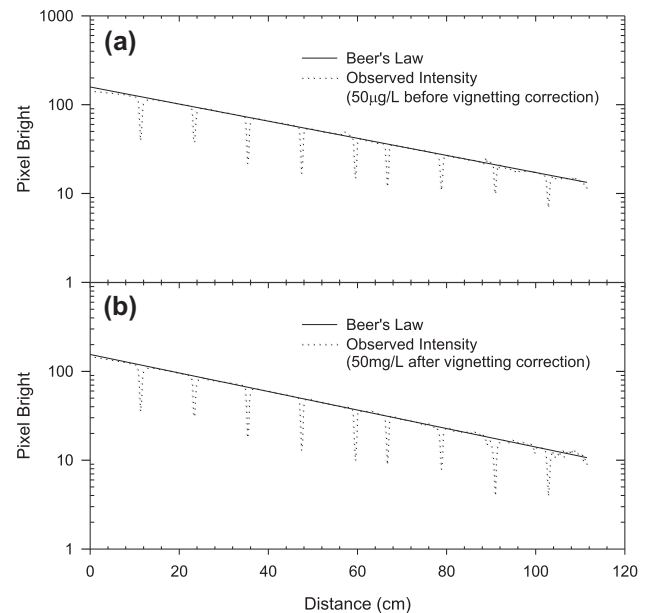


Fig. 3. Laser light attenuation in a model ozone contactor with different Rhodamine 6G, 50 $\mu\text{g/L}$ concentration: (a) before vignetting correction and (b) after vignetting correction.

that two clear peaks appeared from the first to sixth chamber, which was related to the non-ideal flow such as short-circuiting and internal recirculation flow [14]. Although each chamber shared similar hydrodynamics, a noticeable short-circuiting peak appeared on the RTD curves of the first to the fourth chambers, but did not appear on the remaining chambers. A single peak from the sixth chamber implies that the short-circuiting effect

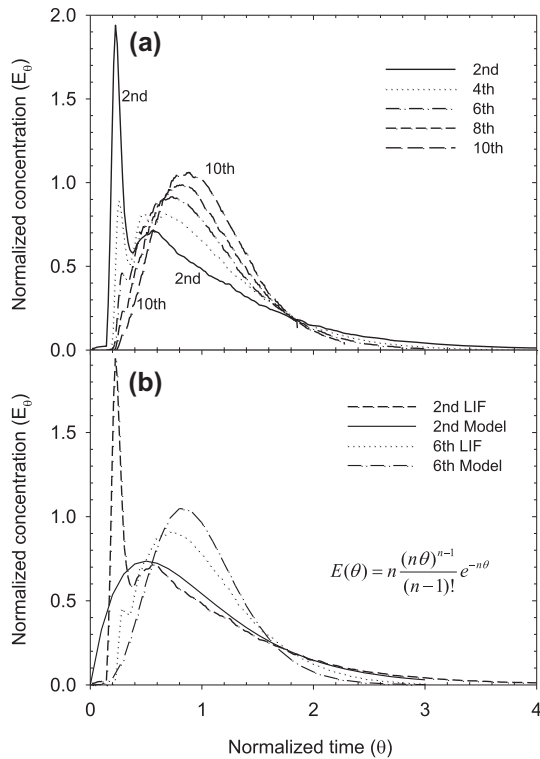


Fig. 4. Non-reactive tracer curve using 3D-LIF system with Rhodamine 6G: (a) tracer curve from second, fourth, sixth, eighth, and tenth chamber and (b) comparison between tracer curve and CSTRs in series model at the second and sixth chamber.

could be almost compensated if the number of ozone chambers was greater than six [18]. The peaks, however, did not match with n -CSTRs in series model as expressed with Eq. (5) because of the non-ideal flow [18]. These flow characteristics will decrease the T_{10} values which are critical for ozone disinfection efficiency [18].

$$E(\theta) = n \frac{(n\theta)^{n-1}}{(n-1)!} e^{-n\theta} \quad (5)$$

where n is the number of chamber in n -CSTRs in series model, E and θ is dimensionless concentration and time, respectively.

3.2. Reproducibility of non-reactive tracer test with 3D-LIF

For the verification of the reproducibility of 3D-LIF system, six non-reactive tracer experiments were carried out with identical experimental conditions at 14 L/min flow. The RTD curve was obtained at the end

of each chamber using 3D-LIF system after pulse-injecting Rhodamine 6G stock solution at the inlet of the model ozone contactor. The RTD curves within 95% confidence level at the second, sixth, and tenth cell are shown in Fig. 5. The reproducibility of RTD curve was shown to be excellent from narrow band width.

Statistical analysis was performed with the RTD results from six duplicate experiments which were done at the same condition. The mean residence time (τ) was compared for the reproducibility, because they were the most frequently used hydrodynamic characteristics of an ozone contactor. The mean residence time was obtained using Eq. (6). The results are shown in Table 1.

$$\tau = \frac{\int_0^{\infty} tCdt}{\int_0^{\infty} Cdt} \approx \frac{\sum_{i=0}^{\infty} t_i C_i \Delta t}{\sum_{i=0}^{\infty} C_i \Delta t} \quad (6)$$

where t and C are time and concentration, respectively. Another measure of experimental reproducibility is the COV. The COV, a measure of the degree of mixing in the reactors, is defined as the ratio of the standard deviation of the tracer concentrations to the mean concentration as shown in Eq. (7):

$$\text{COV} = \frac{\text{Standard Deviation of Tracer Concentrations}}{\text{Mean Tracer Concentration}} = \frac{\sqrt{\frac{1}{n-1} \times \sum_{i,j,k} \left(C(x_i, y_j, z_k, t) - \frac{1}{n} \times \sum_{i,j,k} C(x_i, y_j, z_k, t) \right)^2}}{\frac{1}{n} \times \sum_{i,j,k} C(x_i, y_j, z_k, t)} \quad (7)$$

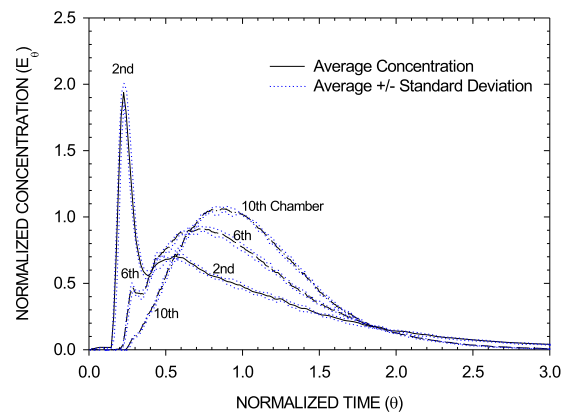


Fig. 5. Reproducibility of non-reactive tracer curve using 3D-LIF system with Rhodamine 6G.

Table 1
The average residence time (τ) of 10 ozone chambers, unit: min

	First	Second	Third	Fourth	Fifth	Sixth	Seventh	Eighth	Ninth	Tenth
1	0.57	1.03	1.44	1.85	2.10	2.52	2.97	3.36	3.77	4.12
2	0.58	1.05	1.45	1.84	2.11	2.52	2.97	3.36	3.77	4.13
3	0.60	1.08	1.49	1.90	2.14	2.56	3.01	3.40	3.81	4.16
4	0.60	1.06	1.49	1.87	2.12	2.53	2.98	3.38	3.78	4.14
5	0.63	1.04	1.48	1.87	2.13	2.54	2.98	3.38	3.79	4.15
6	0.60	1.03	1.47	1.88	2.13	2.55	3.00	3.40	3.81	4.15
Avg.	0.60	1.05	1.47	1.87	2.12	2.54	2.99	3.38	3.79	4.14
Std. dev.	0.02	0.02	0.02	0.02	0.02	0.02	0.02	0.02	0.02	0.01
Skewness	0.34	0.94	-0.66	0.33	-0.41	0.70	0.59	-0.27	0.22	-0.48
COV	0.033	0.018	0.013	0.011	0.007	0.007	0.006	0.005	0.004	0.004

where n is the number of data and i, j , and k are pixel indexes. The COV was the maximum at the first chamber and had the tendency to decrease as the order of chamber increased. The maximum value was 3.3% and the rest were less than this value. From the COV, 3D-LIF system was proved to have excellent reproducibility.

The skewness of mean residence time was randomly distributed and does not show any biased trend for 10 chambers. The skewness (γ^3) is defined as Eq. (8):

$$\gamma^3 = -\frac{\int_0^\infty (t - \bar{t})^3 c dt}{\int_0^\infty c dt} \approx \frac{\sum_{i=0}^{i=\infty} t_i^3 c_i \Delta t}{\sum_{i=0}^{i=\infty} c_i \Delta t} - 3\bar{t}\sigma^2 - \bar{t}^3 \quad (8)$$

The skewness of RTD curve showed randomly positive or negative values because the RTD curve was unbiased. These results also showed very good reproducibility of 3D-LIF system.

Table 2 shows the dispersion numbers (d) of 10 chambers from the six non-reactive tracer tests with pulse injection of non-reactive dye. The average, standard deviation (σ^2), skewness (γ^3), and COV of

the dispersion number were analyzed for each chamber from six experimental results. The highest covariance (COV) of 7% was observed at the second ozone chamber and decreased as the number of the chamber increased. These results showed that conservative tracer tests using 3D-LIF system were very reliable and reproducible for the dispersion number.

3.3. Developing a method for reactive tracer test with nanosized sphere

Pathogen inactivation is affected by ozone concentration and contact time, which are represented as CT in an ozone contactor. As a result of non-ideal flow formed in an ozone contactor, the spatial CT distribution in an ozone contactor would not be uniform. Visualizing CT would be a valuable tool to improve disinfection efficiencies of an ozone contactor because non-ideal flow eventually affects three-dimensional CT distribution in an ozone contactor. Furthermore, the experimental results could be used for verification and calibration of the results from computational fluid dynamics.

Table 2
The dispersion number (d) of 10 ozone chambers

	First	Second	Third	Fourth	Fifth	Sixth	Seventh	Eighth	Ninth	Tenth
1	–	0.73	0.32	0.22	0.18	0.14	0.12	0.10	0.08	0.07
2	–	0.75	0.35	0.22	0.17	0.14	0.12	0.10	0.08	0.07
3	–	0.71	0.34	0.21	0.17	0.14	0.11	0.09	0.08	0.06
4	–	0.79	0.35	0.22	0.17	0.14	0.12	0.10	0.08	0.07
5	–	0.68	0.34	0.22	0.18	0.14	0.12	0.10	0.08	0.07
6	–	0.83	0.33	0.22	0.17	0.14	0.12	0.10	0.08	0.06
Avg.	–	0.75	0.34	0.22	0.17	0.14	0.12	0.10	0.08	0.07
Std. dev.	–	0.05	0.01	0.00	0.00	0.00	0.00	0.00	0.00	0.00
Skewness	–	0.49	-0.67	-1.89	-0.45	-2.02	-0.68	-0.85	-1.62	0.32
COV	–	0.070	0.036	0.018	0.015	0.017	0.013	0.012	0.011	0.013

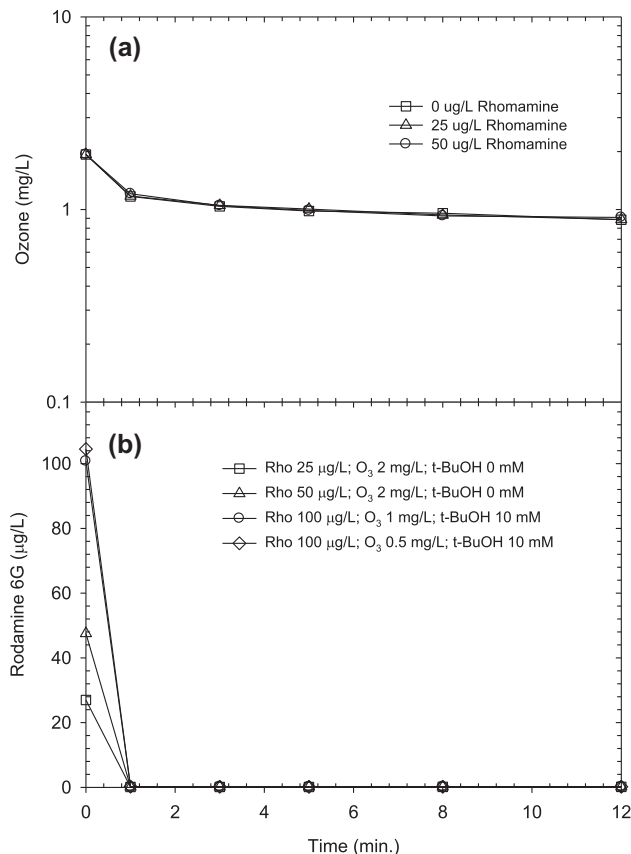


Fig. 6. Ozone (a) and Rhodamine 6G (b) concentration over time.

Rhodamine 6G reacts with ozone and may be considered as a candidate for reactive tracer. Rhodamine 6G, however, instantaneously reacted with ozone which make it inadequate for reactive laser dye. Fig. 6(a) shows the ozone concentration over time with

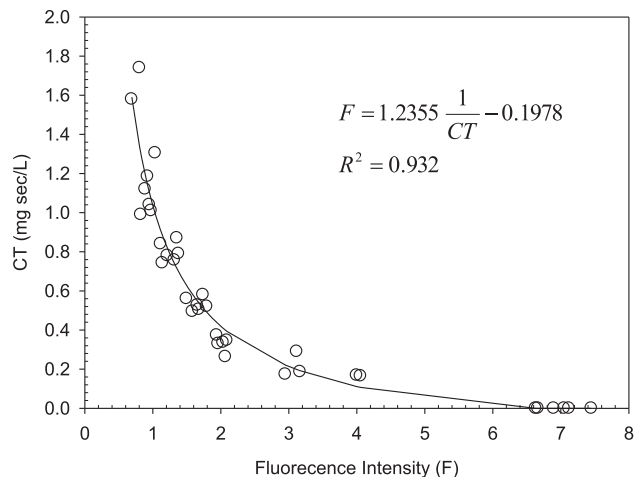


Fig. 7. Relationships between CT and fluorescence intensity.

three Rhodamine 6G concentrations. The ozone concentration profile in this figure was not affected by Rhodamine 6G concentration in the experimental concentration range because Rhodamine 6G reacted so fast that it disappeared regardless of its concentration as shown in Fig. 6(b). Rhodamine 6G primarily reacted with ozone rather than hydroxyl radical since adding t-BuOH did not affect its disappearance.

Dyed microsphere loses color gradually with CT since the dye inside microsphere gradually degraded with ozone over time [19]. Therefore, the dye color intensity could be related with CT in its practical range. Microsphere, however, has the Tyndall effect when it is exposed to laser beam and suffer from extremely high attenuation since microsphere in solution is colloid. We, however, found that nanosized microsphere named Carboxylate Fluoresbrite® YO, 50

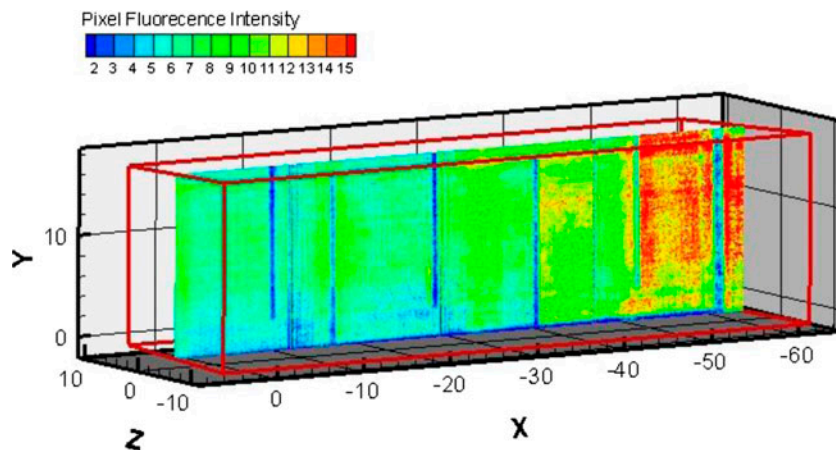


Fig. 8. Fluorescence intensity distribution in the model ozone contactor.

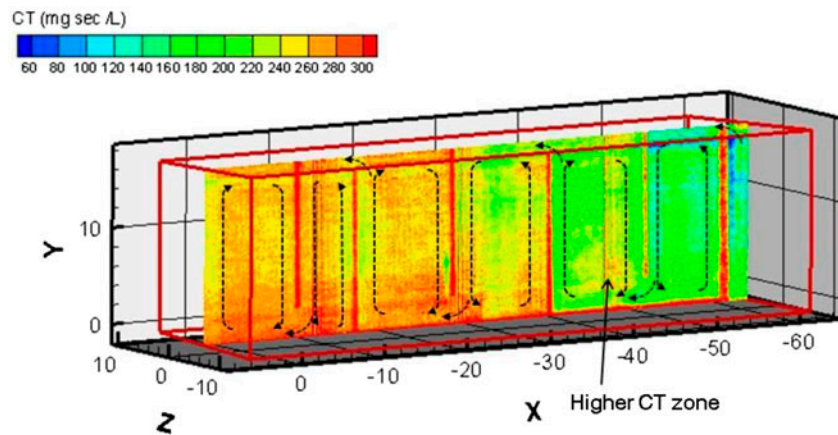


Fig. 9. Actual CT distribution in a model ozone contactor. Note: Dotted lines represent flow direction at each chamber.

nm in diameter, (Polyscience Inc., Warrington, PA) did not have turbidity issues since it was smaller than colloidal size. We found the correlation between fluorescence light intensity and CT as shown in Fig. 7. Fluorescence intensity was inversely proportional to CT in the figure. Fig. 8 is a spatial fluorescence light distribution obtained through the 3D-LIF experiment with the reactive tracer. Fig. 9 is a spatial CT distribution which was converted from Fig. 8 using the equation in Fig. 7. From Fig. 8, we could visualize the actual CT distribution in an ozone contactor at steady state. We can see lower CT in the short-circuiting flow region and higher CT in the internal recirculation zone in the second chambers. Note that low CT is related to the insufficient pathogen inactivation and high CT is related to the elevated carcinogenic bromate formation. The CT distribution, however, was equalized as the number of chamber increased from Fig. 9. This was thought to be caused from lower ozone concentration in those ozone contactors although ozone concentration in each chamber was not measured.

4. Conclusions

Ozone contactor hydrodynamics plays a crucial role in the inactivation efficiency of a pathogen. Effective hydrodynamic design of an ozone contactor is necessary to maintain the safety of drinking water and to save its operational cost. The laser light attenuation followed Beer's law in a model acrylic glass reactor. The non-ideal flow characteristics were shown in the model ozone contactor from tracer curve using non-reactive tracer. It was necessary to make more than six chambers to avoid the non-ideal flow effects in a multi-chambered ozone contactor. The reproducibility and

reliability of 3D-LIF system were proved to be excellent from six duplicate experiments with a non-reactive tracer. The mean residence time and dispersion number were investigated for reproducibility using statistical analysis. Standard deviation, skewness, and COV of them were within superior reproducibility. Reactive tracer test with dyed microsphere successfully showed the spatial actual CT distribution in an model ozone contactor. The results showed that CT distribution in a single chamber was not uniform and affected by non-ideal flow characteristics such as short-circuiting and internal recirculation in each chamber.

Acknowledgments

Dr Roberts in School of Civil and Environmental Engineering, Georgia Institute of Technology is acknowledged for allowing to use the 3D-LIF system. The present research was supported by the research fund from Dankook University in 2012.

References

- [1] L.L. Gyürék, H.B. Li, M. Belosevic, G.R. Finch, Ozone inactivation kinetics of *Cryptosporidium* in phosphate buffer, *J. Environ. Eng.* 125 (1999) 913–924.
- [2] A.M. Driedger, J.L. Rennecker, B.J. Mariñas, Inactivation of *Cryptosporidium parvum* oocysts with ozone and monochloramine at low temperature, *Water Res.* 35 (2001) 41–48.
- [3] B. Corona-Vasquez, J.L. Rennecker, A.M. Driedger, B.J. Mariñas, Sequential inactivation of *Cryptosporidium parvum* oocysts with chlorine dioxide followed by free chlorine or monochloramine, *Water Res.* 36 (2002) 178–188.
- [4] G. Amy, C. Douville, B. Daw, J. Sohn, C. Galey, D. Gatel, J. Cavard, Bromate formation under ozonation

- conditions to inactivate *Cryptosporidium*, Water Sci. Technol. 41 (2000) 61–66.
- [5] J.H. Kim, U. von Gunten, B.J. Mariñas, Simultaneous prediction of *Cryptosporidium parvum* oocyst inactivation and bromate formation during ozonation of synthetic waters, Environ. Sci. Technol. 38 (2004) 2232–2241.
- [6] A. Driedger, E. Staub, U. Pinkernell, B. Mariñas, W. Köster, U. Gunten, Inactivation of *Bacillus subtilis* spores and formation of bromate during ozonation, Water Res. 35 (2001) 2950–2960.
- [7] M. Roustan, C. Beck, O. Wable, J.P. Duguet, J. Mallevalle, Modelling hydraulics of ozone contactors, Ozone Sci. Eng. 15 (1993) 213–226.
- [8] Z. Do-Quang, C.C. Ramirez, M. Roustan, Influence of geometrical characteristics and operating conditions on the effectiveness of ozone contacting in fine-bubbles conventional diffusion reactors, Ozone Sci. Eng. 22 (2000) 369–378.
- [9] M.G. El-Din, D.W. Smith, Development of transient back flow cell model (BFCM) for bubble columns, Ozone Sci. Eng. 23 (2001) 313–326.
- [10] D.J. Greene, B. Farouk, C.N. Haas, CFD design approach for chlorine disinfection processes, J. Am. Water Works Assoc. 96 (2004) 138–150.
- [11] I.A. Hannoun, P.F. Boulos, E.J. List, Using hydraulic modeling to optimize contact time, J. Am. Water Works Assoc. 90 (1998) 77–87.
- [12] G.R. Heathcote, B.E. Drage, Development of an ozone disinfection contactor using a physical scale-model, Ozone Sci. Eng. 17 (1995) 15–24.
- [13] D.J. Henry, E.M. Freeman, Finite element analysis and T-10 optimization of ozone contactors, Ozone Sci. Eng. 17 (1995) 587–606.
- [14] O. Levenspiel, Chemical Reaction Engineering, third ed., John Wiley & Sons, New York, NY, 1999.
- [15] J.H. Kim, M.S. Elovitz, U. von Gunten, H.M. Shukairy, B.J. Mariñas, Modeling *Cryptosporidium parvum* oocyst inactivation and bromate in a flow-through ozone contactor treating natural water, Water Res. 41 (2007) 467–475.
- [16] X.D. Tian, P.J.W. Roberts, A 3D LIF system for turbulent buoyant jet flows, Exp. Fluids 35 (2003) 636–647.
- [17] L. Kong, J. Zhu, C. Zhang, Catalytic ozone decomposition in a gas–solids circulating fluidized-bed riser, Chem. Eng. Technol. 37 (2014) 435–444.
- [18] D. Kim, T. Stoesser, J.H. Kim, The effect of baffle spacing on hydrodynamics and solute transport in serpentine contact tanks, J. Hydraul. Res. 51 (2013) 558–568.
- [19] G. Tang, K. Adu-Sarkodie, D. Kim, J.H. Kim, S. Teefy, H.M. Shukairy, B.J. Mariñas, Modeling *Cryptosporidium parvum* oocyst inactivation and bromate formation in a full-scale ozone contactor, Environ. Sci. Technol. 39 (2005) 9343–9350.